AGU PUBLICATIONS

Geophysical Research Letters

RESEARCH LETTER
10.1002/2016GL070953

Key Points:
- Novel observation-based climatology of MODIS aerosol optical depth in extratropical cyclones
- Link between AOD and air flows within ETCs clearly observed, with two different ingestion regions
- Observed coarse mode aerosols predominant in warm sector, fine mode aerosols predominant in cold sector

Correspondence to:
C.M. Naud,
cn2140@columbia.edu

Citation:
Naud, C. M., D. J. Posselt, and S. C. van den Heever (2016), Aerosol optical depth distribution in extratropical cyclones over the Northern Hemisphere oceans, *Geophys. Res. Lett.*, *43*, 10,504–10,511, doi:10.1002/2016GL070953.

Received 22 AUG 2016
Accepted 27 SEP 2016
Accepted article online 30 SEP 2016
Published online 11 OCT 2016

Aerosol optical depth distribution in extratropical cyclones over the Northern Hemisphere oceans

Catherine M. Naud[1], Derek J. Posselt[2], and Susan C. van den Heever[3]

[1]NASA-GISS, Columbia University, New York, New York, USA, [2]Jet Propulsion Laboratory, California Institute of Technology, Pasadena, California, USA, [3]Department of Atmospheric science, Colorado State University, Fort Collins, Colorado, USA

Abstract Using Moderate Resolution Imaging Spectroradiometer and an extratropical cyclone database, the climatological distribution of aerosol optical depth (AOD) in extratropical cyclones is explored based solely on observations. Cyclone-centered composites of aerosol optical depth are constructed for the Northern Hemisphere midlatitude ocean regions, and their seasonal variations are examined. These composites are found to be qualitatively stable when the impact of clouds and surface insolation or brightness is tested. The larger AODs occur in spring and summer and are preferentially found in the warm frontal and in the postcold frontal regions in all seasons. The fine mode aerosols dominate the cold sector AODs, but the coarse mode aerosols display large AODs in the warm sector. These differences between the aerosol modes are related to the varying source regions of the aerosols and could potentially have different impacts on cloud and precipitation within the cyclones.

1. Introduction

Up to 90% of the rainfall in storm track regions is produced by fronts associated with extratropical cyclones (ETCs) [*Catto et al*., 2012]. While observation- and modeling-based studies have provided insight into the mechanisms that control the amount, intensity, and distribution of rainfall in midlatitude storms, significant questions remain about the cloud and precipitation response to changes in environmental aerosol. Recent studies have utilized models to examine the sensitivity of frontal liquid and ice clouds [*Igel et al*., 2013; *Thompson and Eidhammer*, 2014; *Lu and Deng*, 2016] and postcold frontal clouds [*Sheffield and van den Heever*, 2014; *Sheffield*, 2016], to variations in aerosol loading. These modeling studies have revealed complex aerosol-cloud feedbacks that depend on cloud phase and the region of the storm into which aerosols are chosen to be introduced. As such, there is a critical need to examine, from an observational perspective, the distribution of aerosol mass, number, and type around extratropical cyclones. The goal of this study is therefore to examine how aerosols are distributed within and around extratropical cyclones and how this distribution changes with season and with the type of aerosols being transported.

While previous observational studies have examined composites of observed cloud features in and around ETCs [e.g., *Evans et al*., 1994; *Lau and Crane*, 1995, 1997; *Klein and Jakob*, 1999; *Tselioudis et al*., 2000; *Naud et al*., 2006, 2010, 2012, 2013, 2015; *Field and Wood*, 2007; *Field et al*., 2008; *Bender et al*., 2012], a search of the literature reveals only a few observational studies of the climatological aerosol distribution around ETCs [*Grandey et al*., 2011, 2013]. In the current study we utilize a 4 year database of Moderate Resolution Imaging Spectroradiometer (MODIS)-retrieved aerosol optical depth (AOD) and type, in concert with a set of objectively identified cyclone centers, to examine the composite distribution of aerosol around ETCs in the Northern Hemisphere oceanic cyclones. We explore the sensitivity of our results to cloud cover and latitude and subset the composite to examine different regions and seasons. Finally, we examine the distribution of AOD for the three main modes of aerosols as defined in the MODIS retrieval algorithm: a fine mode and two coarse modes here referred to as "sea salt like" and "dust like." This research therefore provides a detailed description of the *observed* climatological distribution of aerosols in ETCs and thus serves as an observational constraint for modeling studies. It also provides a foundation for future, more detailed studies of the regional effect of aerosols on ETCs, as well as the connection between aerosols and storm development life cycle.

2. Data

To obtain information on aerosol optical depth over oceans, we use the daily *Aqua* Moderate Resolution Imaging Spectroradiometer (MODIS) [*Salomonson et al*., 1989] Collection 6 aerosol optical depth retrievals

[*Levy et al.*, 2013]. We use the combined quality-controlled product referred to as "Optical_depth_land_and_ocean" [*Levy et al.*, 2013]. Over oceans, aerosol optical depth (AOD) is retrieved by comparing measured top-of-atmosphere reflectances at seven wavelengths to a lookup table of precomputed reflectances [*Remer et al.*, 2005]. These 250 or 500 m resolution (depending on wavelength) reflectances are all mapped to a 500 m resolution grid before cloud clearing tests are applied. The *cloud-free* 500 m reflectances are then averaged in 10 km × 10 km pixels if at least 10 are available out of 400. Thus, for any given 10 km pixel, there can be an AOD retrieval even if cloud cover $> 0\%$. The MODIS lookup table assumes nine possible tropospheric aerosol modes [*Levy et al.*, 2003]: four fine modes (effective radii R_{eff} 0.1, 0.15, 0.2, and 0.25 μm) dominated by chemical and combustion processes and five coarse modes dominated by maritime particles (R_{eff} 1, 1.5, and 2 μm) and mineral dust (R_{eff} 1.5 and 2.5 μm). From the daily files we extract the total AOD for all modes and per mode, reported in a 1° × 1° grid, for September 2006 to August 2010. These products were evaluated by *Remer et al.* [2008] and more recently by *Levy et al.* [2013]. Known issues include errors caused by surface snow and ice, sun glint, and clouds. *Remer et al.* [2008] had previously reported a tendency for AODs to be twice the global mean in 10 km areas with cloud cover exceeding 80% and that the cloud masking routine was subsequently improved for the latest processing of the MODIS data set. We will test how these potential retrieval errors might impact our results. Misidentification of snow and ice, and low insolation, might also affect our results, so this will also be evaluated.

Cyclone locations are available every 6 h in the NASA Modeling, Analysis and Prediction Climatology of Midlatitude Storminess (MCMS) database [*Bauer et al.*, 2016]. The MCMS algorithm detects and tracks local minima in the 6-hourly ERA-interim [*Dee et al.*, 2011] sea level pressure field. The 6-hourly locations of the storm centers found in the Northern Hemisphere oceans are collected for the period September 2006 to August 2010. Even though the aerosol properties are reported as daily averages, they are in fact acquired once a day at each point on Earth (1:30 pm equator crossing time). To ensure a consistent match in time between daily AODs and 6-hourly ETCs, we only select those cyclone centers that are found within ±3 h and 25° from the Aqua orbits. Consequently, the results are a once-per-day snapshot and do not take into account any possible daily variability. Over a 4 year period, this approach results in a database of 21,822 cyclones in the Northern Hemisphere oceans, ~8000 cyclones in the Atlantic versus ~12,000 cyclones in the Pacific Ocean.

3. Results

First we examine the seasonal MODIS AOD distribution in the Northern Hemisphere midlatitudes (30–60°N) and the coincident cyclone center distributions. To facilitate direct comparison between AOD and the cyclone distributions, we choose to count the number of cyclone centers in 5° × 5° grid cells to produce climatological maps. This choice of grid cell size is rather arbitrary and is intended to strike a balance between sufficient cyclone density in each cell and sufficient resolution to properly represent the spatial distribution of the cyclones. Halving or doubling the grid cell length would change the number of storms in each grid box but would not fundamentally change our results. Figure 1 shows the maps for both AODs and cyclone numbers per season defined as December–February (DJF), March–May (MAM), June–August (JJA), and September–November (SON). Figure 1 demonstrates that (1) the largest AODs over the oceans are found in spring and summer, with greater values and a wider spatial spread in the Pacific than the Atlantic Oceans; (2) the lowest AODs are found in winter and fall, with lower values close to the polar circle and south of the storm tracks; and (3) the maps do not reveal a clear coincidence between the cyclone locations and the large AODs over the Atlantic, but in the Pacific, especially in spring and summer, there might be a correspondence between large number of cyclones and large AOD. These maps seem to suggest that given the coincidence between cyclone location and AODs, the AODs within cyclones will be larger in spring and summer than in the other two seasons and are likely to be greater over the Pacific Ocean.

To verify this, we composited AODs in a region of 25° radius in size and centered on the cyclone low pressure centers, separately for each season. All cyclones in our database, in both ocean basins during the 4 year period, are included regardless of strength, age, latitude, ocean basin, or synoptic characteristics. These composites are obtained by regridding the AOD data coincident with each cyclone into an identical stereographic grid centered on the low, and averaging all superimposed cyclones AODs, as described in *Naud et al.* [2012]. Figures 2a–2d show these composites of Northern Hemisphere (NH) ocean cyclone-centered AODs per

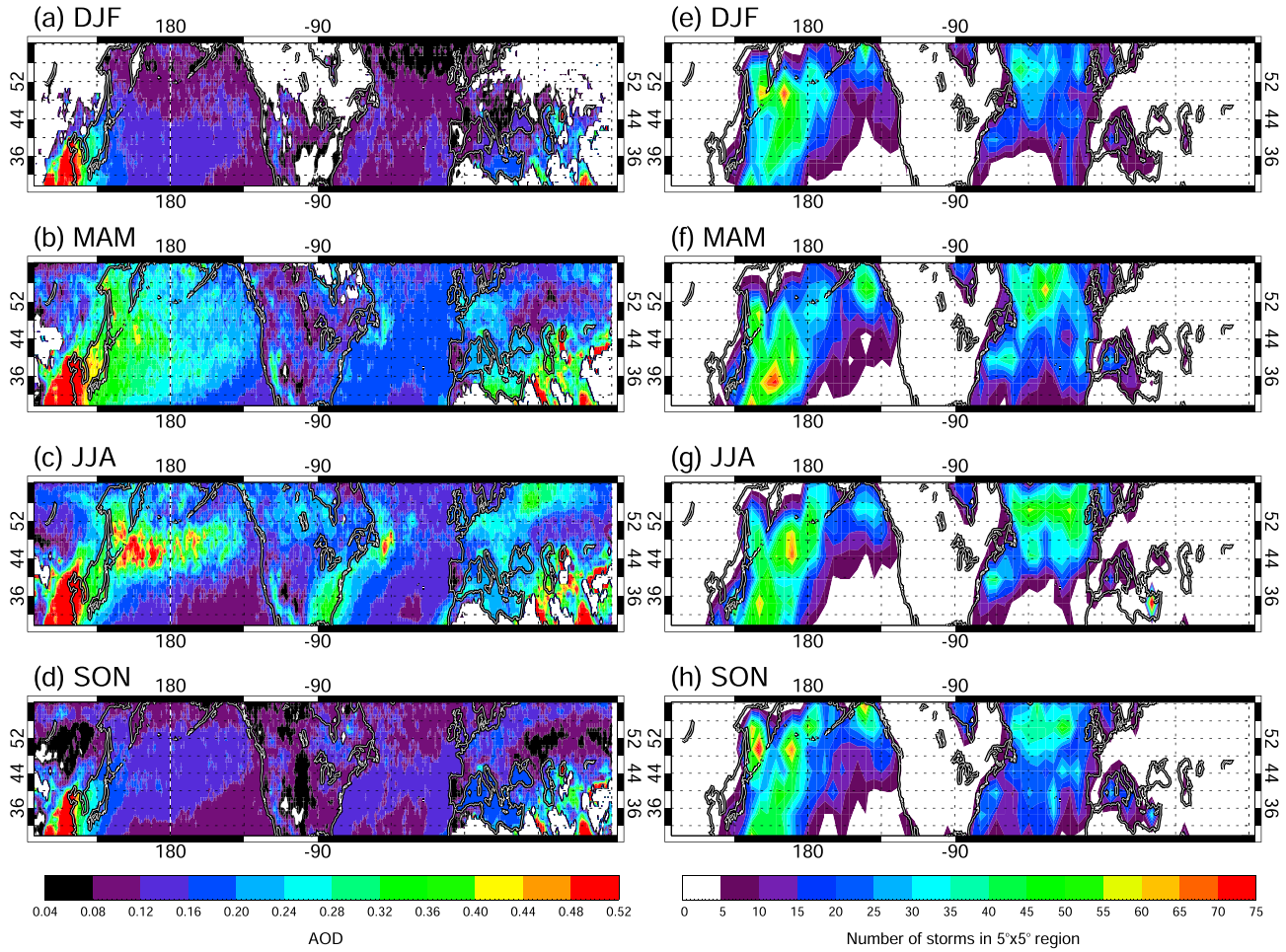

Figure 1. Northern Hemisphere midlatitude (30–70°N) seasonal mean of MODIS AOD and cyclone locations over oceans, for (a, e) DJF, (b, f) MAM, (c, g) JJA, and (d, h) SON for 2006–2010.

season focusing on the region ±1500 km east/west and north/south of the center of the cyclones. It confirms that indeed the spring and summer cyclone-centered AODs are larger than in winter and fall. Furthermore, all seasons exhibit two regions of relatively large AOD within the cyclones, i.e., warm frontal and postcold frontal regions, and two relative minima, one in the cold sector to the north/north-east of the low and the other on the equator edge of the cyclonic region, to the south/south-east of the low. Overall, Figure 2 suggests that aerosols in cyclones are concentrated in regions from which they can be transported either poleward and upward in the warm conveyor belt or equatorward, downward, and eastward in the northwesterly circulation behind cold fronts.

As mentioned earlier, one major issue when retrieving aerosol optical depth is cloud contamination. We calculate the mean cyclone-centered AOD using only those pixels with a collocated cloud fraction less than 80% for each cyclone (53% of all AOD data points). In addition, retrievals are missing in regions with insufficient insolation and over bright surfaces such as snow and sea ice. Here we calculate the mean cyclone-centered AOD by reducing the latitude range from 30–60°N to 30–50°N in an attempt to remove both insolation and surface brightness issues. Figures 2e–2h show the cyclone-centered composites of AODs obtained where cloud cover is less than 80%, and Figures 2i–2l show the composites for cyclones with a center within 30–50°N rather than 30–60°N. Figures 2e–2h demonstrate that the mean AODs decrease when cloud cover is less than 80%, consistent with *Remer et al.*'s [2008] results, but that this happens rather uniformly within the cyclone area and across seasons. Table 1 gives the mean difference in cyclone mean AOD between composites using all retrievals and composites using only retrievals where total cloud cover (TCC) $< 80\%$. Both the bias and the correlation coefficient across the composite were evaluated. The latter gives an indication on how

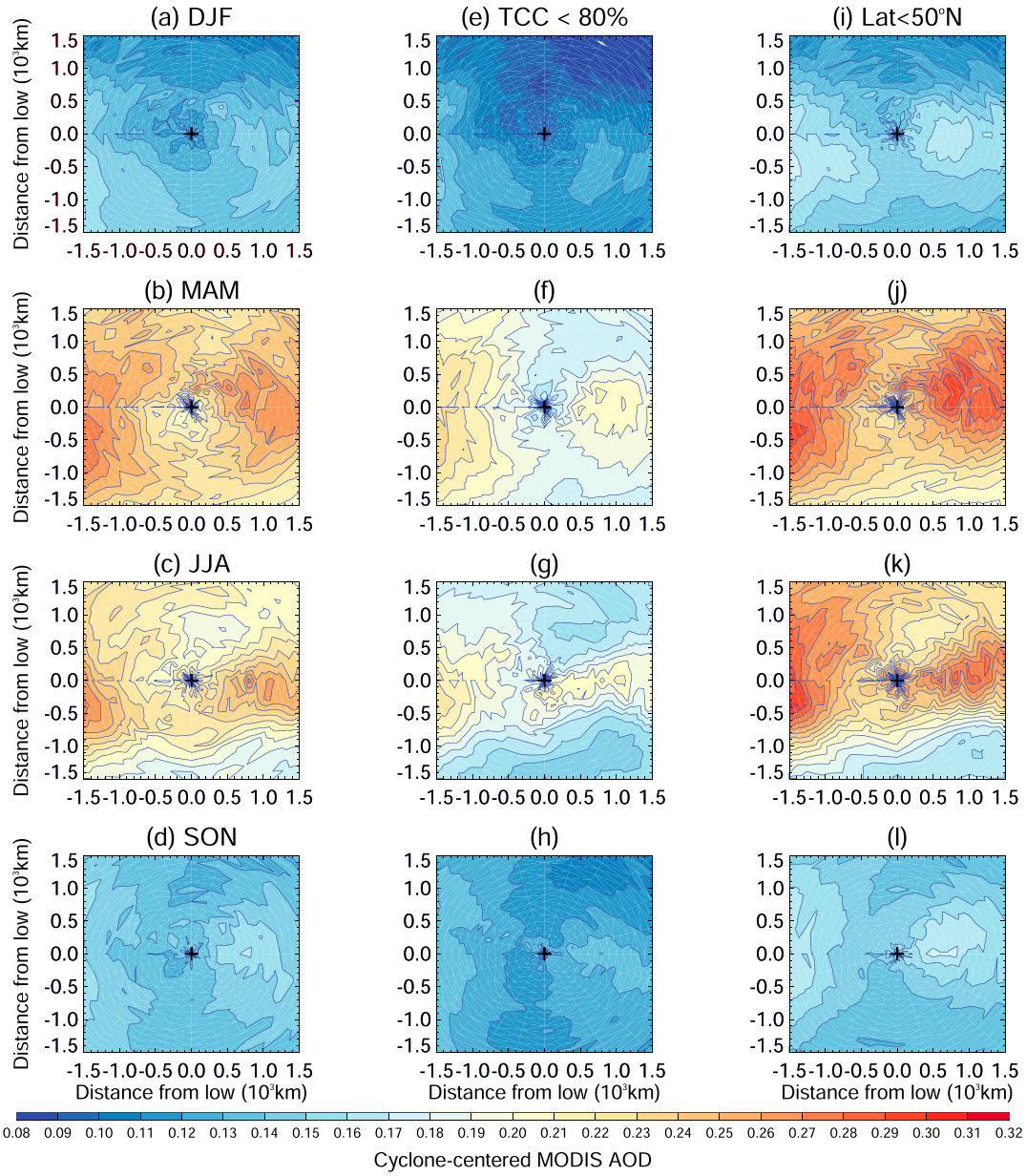

Figure 2. Cyclone-centered composites of MODIS AOD for all retrievals, retrievals where cloud cover < 80% and cyclones south of 50°N for (a–c) winter (DJF), (d–f) spring (MAM), (g–i) summer (JJA), and (j–l) fall (SON).

spatially variable the bias might be. The largest impact of cloud cover is found in the spring, and the lowest in the fall, but the reduction in AOD is proportionally similar across seasons (around 15%). The correlation coefficients also suggest a rather uniform impact. Next we examine the mean cyclone-centered AODs when considering only cyclones with a center south of 50°N to alleviate the impact of missing retrievals caused by bright surfaces and low insolation. Figures 2i–2l show an increase in AOD across the cyclones for all four seasons when compared with the composites obtained with the entire database. Table 1 also shows how this subset differs from the full set. By removing the northernmost cyclones, we sample less of the regions with low AODs, and hence, the overall mean AOD increases within the cyclones, for all seasons. Because of the lack of seasonality, this effect seems to dominate over missing retrievals in winter. The relative maxima and minima remain, and, as shown in Table 1, the correlations are large and the biases small. Consequently, we find that, qualitatively at least, the impact of missing retrievals on the cyclone-centered AOD is small.

Table 1. Comparison Between Cyclone-Centered Composites of MODIS AOD Using All Retrievals and Composites Using Only Total Cloud Cover TCC < 80% or Latitudes of Cyclones South of 50°N: Correlation Coefficient for 25 × 25 Pixels in the Composites and Mean With Standard Deviation of the Difference Between All Retrievals and Either Subsets

	Correlation Coefficient		Mean Bias	
Season	TCC < 80%	Latitude < 50°N	TCC < 80%	Latitude < 50°N
Winter	0.91	0.85	0.02 ± 0.01	−0.01 ± 0.01
Spring	0.81	0.87	0.05 ± 0.02	−0.01 ± 0.02
Summer	0.88	0.86	0.04 ± 0.02	−0.02 ± 0.02
Fall	0.93	0.90	0.02 ± 0.01	−0.01 ± 0.01

Next we separate the aerosols according to the nine MODIS specific aerosol modes [*Levy et al*., 2003]. Table 2 gives the mean AOD per cyclone per season for each mode. Amongst the four fine particle modes, the largest cyclone-wide mean AOD is found for the finest (R_{eff} = 0.1 μm) mode in summer and fall, while the coarsest mode (R_{eff} = 0.25 μm) dominates in winter and spring. Overall, the fine modes exhibit significantly larger AODs than the coarse modes. For simplicity, we combine the AODs of the fine modes together and do the same for the three sea-salt-like modes and the two dust-like modes. We then explore where in the cyclones these three general modes of aerosols are found by examining the mean cyclone-centered AOD per aerosol mode (Figures 3a–3c). The fine modes exhibit much larger AODs than the sea-salt-like modes, while the dust-like modes exhibit the lowest AODs. This is consistent with *Remer et al*. [2008] who report relatively low dust AODs over oceans. The fine AOD modes achieve a maximum in the cold sector of the cyclones, while the coarse modes show a relative maximum in the warm sector and cold frontal region. This suggests that the fine modes, which mostly comprise chemical and combustion types of aerosol, are ingested in the equatorward, downward, and eastward northwesterly circulation behind cold fronts. Figure 3b is consistent with the conclusions of *Grandey et al*. [2011] who find that sea salt dominates AOD in the region of the cyclones where wind speed is maximum, suggesting that sea salt is in fact emitted and lifted by the wind flow of the cyclones themselves. Finally, Figure 3c indicates that dust-like aerosols are ingested into the cyclone mostly in the warm conveyor belt, which is consistent with the global MODIS dust AOD distribution over oceans that show a maximum in the subtropics.

To get a better sense of how much of each aerosol mode contributes to the total cyclone AOD, the percentage of the total AOD that is contributed by each of the three AOD modes was calculated. Figures 3d–3f show the cyclone-centered percentages for the fine, the sea-salt-like, and the dust-like modes. These figures demonstrate that the cold sector is dominated by the fine mode but that in the warm sector the fine and sea-salt-like modes make similar contributions of around 40–45% of the total AOD. Mineral dust-like modes tend to be a maximum in a region resembling the cold frontal/warm conveyor belt area.

As the AOD distributions differ greatly between the two oceans (Figure 1), the Atlantic and Pacific cyclones are examined separately to determine whether the nature of the aerosols differs between the two ocean basins. Figures 3g–3i show the composites for the Atlantic and Figures 3j–3l for the Pacific Ocean. The contribution of the fine mode AOD is much larger in the Pacific than in the Atlantic, while the contribution of dust-like AOD is larger in the Atlantic than in the Pacific. The contribution of the sea-salt-like AOD to the total AOD is more uniform across the cyclone region in the Atlantic than in the Pacific and tends to spread into the

Table 2. Mean MODIS AOD per Cyclone-Centered Composite and per Aerosol Mode Over the Midlatitude Northern Hemisphere Oceans for the Entire Period and for Winter, Spring, Summer, and Fall

	Aerosol Modes								
	Fine Mode				Sea Salt Like			Mineral Dust Like	
Cyclone Sets	R_{eff} = 0.1 μm	R_{eff} = 0.15 μm	R_{eff} = 0.2 μm	R_{eff} = 0.25 μm	R_{eff} = 1 μm	R_{eff} = 1.5 μm	R_{eff} = 2 μm	R_{eff} = 1.5 μm	R_{eff} = 2.5 μm
All	0.046	0.022	0.020	0.034	0.026	0.019	0.033	0.001	0.009
Winter	0.027	0.017	0.018	0.030	0.024	0.019	0.028	0.002	0.004
Spring	0.056	0.029	0.027	0.057	0.039	0.025	0.037	0.001	0.010
Summer	0.064	0.025	0.020	0.031	0.024	0.020	0.043	0.001	0.012
Fall	0.037	0.018	0.017	0.023	0.018	0.015	0.025	0.001	0.008

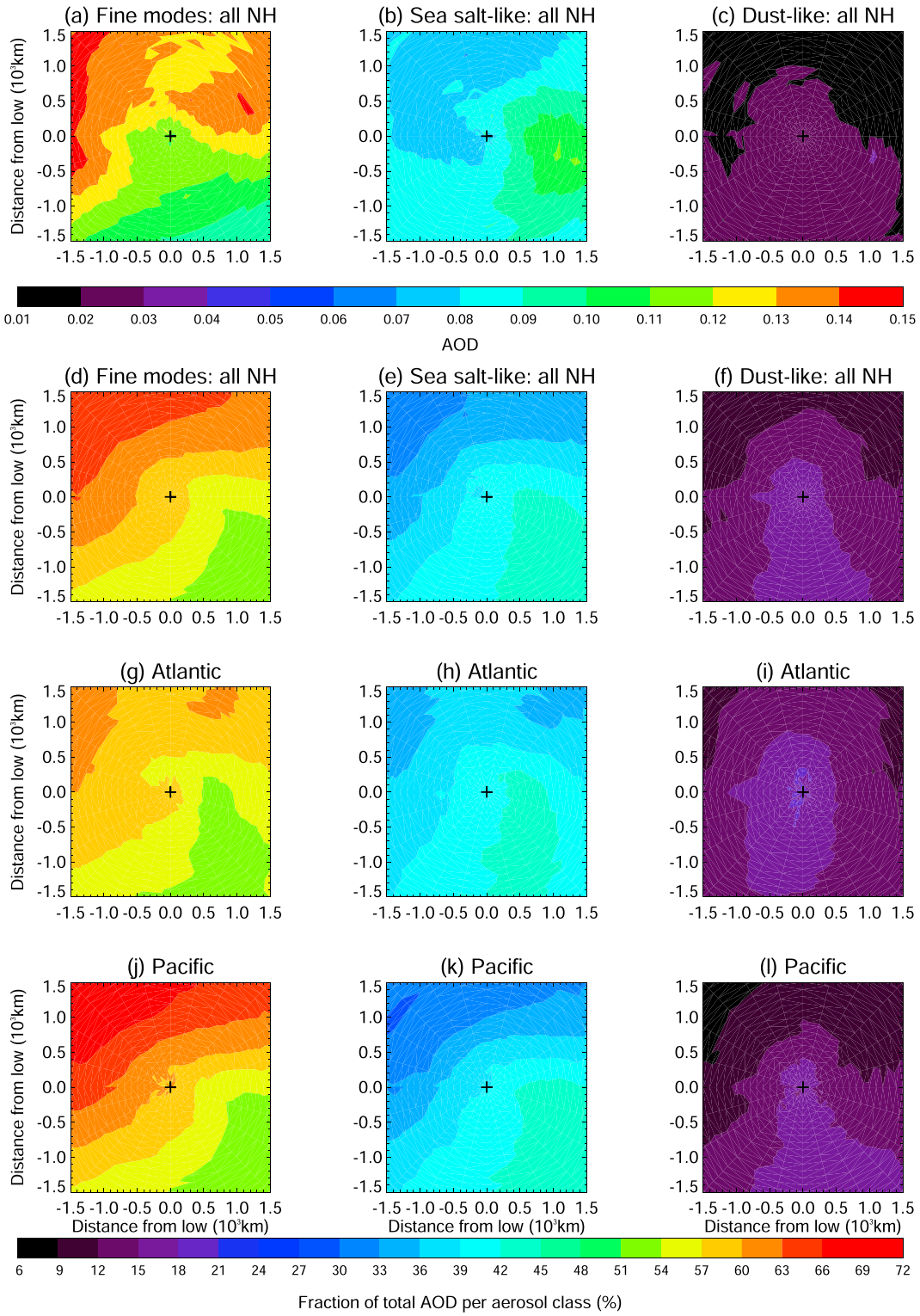

Figure 3. Cyclone-centered AOD for all oceanic midlatitude Northern Hemisphere (NH) cyclones for (a) fine, (b) sea-salt-like, and (c) mineral dust-like modes. Cyclone-centered composites of the fraction of the total AOD contributed by (d, g, j) fine, (e, h, k) sea-salt-like modes, and (f, i, l) dust-like modes for all NH (Figures 3d–3f), Atlantic (Figures 3g–3i), and Pacific cyclones (Figures 3j–3l).

cold sector more extensively than it does in the Pacific. As various aerosol types serve differently as cloud condensation or ice nuclei, these results can help in predicting the type of hydrometeors that might be activated in different locations of the storm. Also, different aerosol types have varying absorptive capabilities, and thus, these results could also help to assess whether thermodynamically stable layers are present in different regions in and around the cyclones.

4. Conclusions

Using MODIS aerosol optical depth (AOD) retrievals and a database of extratropical cyclone locations, we have examined for the first time the distribution of aerosols within extratropical cyclones found in the Northern Hemisphere oceans. In the Northern Hemisphere oceans, the AOD is largest in spring and summer. Within the cyclones, composites of AOD reveal that there are two areas of relative maximum AOD, one in the warm frontal zone and the other to the west of the low in the cold sector. This spatial distribution changes little with season, cloud cover, or latitude. However, the magnitude of AOD increases with cloud cover, increases with decreasing latitude, and is largest in spring and summer. When examining the nine MODIS aerosol-type AOD distributions within the cyclones, we found a dominance of the fine mode in the entirety of the cold sector and an equal occurrence of the fine modes and sea-salt-like modes in the warm sector. The dust-like modes exhibit much lower AODs within the cyclones, consistent with the low dust AODs found more generally over oceans [e.g., *Remer et al*., 2008].

These results are a first attempt at exploring a climatology of aerosols within extratropical cyclones using only satellite observations. However, there are some caveats as follows: (1) aerosols cannot be retrieved if clouds are present which casts some doubts on the accuracy of AODs close to the storm centers and in the warm frontal region (see *Naud et al*. [2013] for the cloud cover distribution in cyclones), and (2) the different modes used for aerosol AOD retrievals are not entirely physically based even though the refractive indices are, as all particles, including dust, are assumed to be spherical [*Levy et al*., 2003]. One question raised by Figure 3 is whether the coarse mode signal is obscured by the fine mode signal in the reflectances measured by MODIS and whether this is the reason for the relative maximum in the coarse modes AOD in the warm sector where the fine mode AOD is minimum. Another question is whether MODIS retrievals can truly separate the sea-salt and dust mode signals. Finally, other possible shortfalls are that along the coastal regions, some of the AOD retrievals might be performed over land where there are larger uncertainties in particle size and that the sun glint problem might affect the southernmost cyclones AOD [*Remer et al*., 2008].

Despite these caveats, the implications of these results are as follows:

1. The regions with large AODs also coincide with regions that are known to be critical for the formation of frontal clouds and hence may influence frontal precipitation, as suggested by previous modeling studies [*Igel et al*., 2013; *Thompson and Eidhammer*, 2014; *Lu and Deng*, 2016].
2. The warm conveyor belt within the warm sector ascends throughout the depth of the troposphere and is known to have nearly 100% precipitation efficiency [*Boutle et al*., 2011]. The presence of aerosols within this region may therefore have impacts on the precipitation efficiency within this conveyor belt.
3. Aerosols in the postcold frontal region can potentially interact with shallow convection [*Sheffield and van den Heever*, 2014]. Recent studies have shown that many of these postcold frontal cumulus clouds in these regions precipitate [*Naud et al*., 2015], and hence, they might be especially susceptible to changes in aerosol concentrations.

Consequently, the next step in this research will be to examine the relationship between AOD and cloud properties in cyclones and how this might impact precipitation. Also, in view of the apparent aerosol distribution differences between the two NH ocean basins, we will focus more closely on their potential disparities in terms of the aerosol distribution and its impact on cloud and precipitation in extratropical cyclones.

Acknowledgments
Funding for this study comes from NASA CloudSat science team recompete grant NNX13AQ33G. The MCMS extratropical cyclone data set, algorithm, and documentation are available at http://gcss-dime.giss.nasa.gov/mcms/. The MODIS Aqua collection 6 daily MYD08_D3 files were obtained from the Level 1 and Atmosphere Archive and Distribution system at the Goddard Space Flight https://ladsweb.nascom.nasa.gov. The authors thank two anonymous reviewers for their helpful comments.

References

Bauer, M. P., G. Tselioudis, and W. B. Rossow (2016), A new climatology for investigating storm influences in and on the extratropics, *J. Appl. Meteorol. Climatol.*, *55*, 1287–1303.

Bender, F. A.-M., V. Ramanathan, and G. Tselioudis (2012), Changes in extratropical storm track cloudiness 1983–2008: Observational support for a poleward shift, *Clim. Dyn.*, *38*, 2037–2053.

Boutle, I. A., S. E. Belcher, and R. S. Plant (2011), Moisture transport in midlatitude cyclones, *Q. J. R. Meteorol. Soc.*, *137*, 360–373.

Catto, J. L., C. Jakob, G. Berry, and N. Nicholls (2012), Relating global precipitation to atmospheric fronts, *Geophys. Res. Lett.*, *39*, L10805, doi:10.1029/2012GL051736.

Dee, D. P., et al. (2011), The ERA-Interim reanalysis: Configuration and performance of the data assimilation systems, *Q. J. R. Meteorol. Soc.*, *137*, 553–597.

Evans, M. S., D. Keyser, L. F. Bosart, and G. M. Lackmann (1994), A satellite-derived classification scheme for rapid maritime cyclogenesis, *Mon. Weather Rev.*, *122*, 1381–1416.

Field, P. R., A. Gettelman, R. B. Neale, R. Wood, P. J. Rasch, and H. Morrison (2008), Midlatitude cyclone compositing to constrain climate model behavior using satellite observations, *J. Clim.*, *21*, 5887–5903.

Field, P. R., and R. Wood (2007), Precipitation and cloud structure in midlatitude clouds, *J. Clim.*, *20*, 233–254 Corrigendum, 20, 5208–5210.

Grandey, B. S., P. Stier, T. M. Wagner, R. G. Grainger, and K. I. Hodges (2011), The effect of extratropical cyclones on satellite retrieved aerosol properties over ocean, *Geophys. Res. Lett.*, *38*, L13805, doi:10.1029/2011GL047703.

Grandey, B. S., P. Stier, R. G. Grainger, and T. M. Wagner (2013), The contribution of the strength and structure of extratropical cyclones to observed cloud-aerosol relationships, *Atmos. Chem. Phys.*, *13*, 10,689–10,701, doi:10.5194/acp-13-10689-2013.

Igel, A. L., S. C. van den Heever, C. M. Naud, S. M. Saleeby, and D. J. Posselt (2013), Sensitivity of warm-frontal processes to cloud-nucleating aerosol concentrations, *J. Atmos. Sci.*, *70*, 1768–1783.

Klein, S. A., and C. Jakob (1999), Validation and sensitivities of frontal clouds simulated by the ECMWF model, *Mon. Weather Rev.*, *127*, 2514–2531.

Lau, N.-C., and M. W. Crane (1995), A satellite view of the synoptic-scale organization of cloud properties in midlatitude and tropical circulation systems, *Mon. Weather Rev.*, *123*, 1984–2006.

Lau, N.-C., and M. W. Crane (1997), Comparing satellite and surface observations of cloud patterns in synoptic-scale circulation systems, *Mon. Weather Rev.*, *125*, 3172–3189.

Levy, R. C., L. A. Remer, D. Tanré, Y. J. Kaufman, C. Ichoku, B. N. Holben, J. M. Linvingston, P. B. Russell, and H. Maring (2003), Evaluation of the Moderate-Resolution Imaging Spectroradiometer (MODIS) retrievals of dust aerosol over the ocean during PRIDE, *J. Geophys. Res.*, *108*(D19), 8594, doi:10.1029/2002JD002460.

Levy, R. C., S. Mattoo, L. A. Munchak, L. A. Remer, A. M. Sayer, F. Patadia, and N. C. Hsu (2013), The collection 6 MODIS aerosol products over land and ocean, *Atmos. Meas. Tech.*, *6*, 2989–3034, doi:10.5194/amt-6-2989-2013.

Lu, Y., and Y. Deng (2016), Impact of environmental aerosols on a developing extratropical cyclone in the superparameterized Community Atmosphere Model, *J. Clim.*, *29*, 5533–5546.

Naud, C. M., A. D. Del Genio, and M. Bauer (2006), Observational constraints on cloud thermodynamic phase in midlatitude storms, *J. Clim.*, *19*, 5273–5288, doi:10.1175/JCLI3919.1.

Naud, C. M., D. J. Posselt, and S. C. van den Heever (2012), Observational analysis of cloud and precipitation in midlatitude cyclones: Northern versus southern hemisphere warm fronts, *J. Clim.*, *25*, 5135–5151.

Naud, C. M., J. F. Booth, D. J. Posselt, and S. C. van den Heever (2013), Multiple satellite observations of cloud cover in extratropical cyclones, *J. Geophys. Res. Atmos.*, *118*, 9982–9996, doi:10.1002/jgrd.50718.

Naud, C. M., A. D. Del Genio, M. Bauer, and W. Kovari (2010), Cloud vertical distribution across warm and cold fronts in CloudSat-CALIPSO data and a general circulation model, *J. Clim.*, *23*, 3397–3415, doi:10.1175/2010JCLI3282.1.

Naud, C. M., D. J. Posselt, and S. C. van den Heever (2015), A CloudSat-CALIPSO view of cloud and precipitation properties across cold fronts over the global oceans, *J. Clim.*, *28*, 6743–6762, doi:10.1175/JCLI-D-15-0052.1.

Remer, L. A., et al. (2005), The MODIS aerosol algorithm, products, and validation, *J. Atmos. Sci.*, *62*, 947–973.

Remer, L. A., et al. (2008), Global aerosol climatology from the MODIS satellite sensors, *J. Geophys. Res.*, *113*, D14S07, doi:10.1029/2007JD009881.

Salomonson, V. V., W. L. Barnes, P. W. Maymon, H. E. Montgomery, and H. Ostrow (1989), MODIS: Advanced facility instrument for studies of the Earth as a system, *IEEE Trans. Geosci. Remote Sens.*, *27*, 145–153.

Sheffield, A. M., and S. C. van den Heever (2014), Aerosol impacts on post-cold frontal cumulus clouds and the extratropical cyclone moisture budget, AMS Cloud Physics Conference, 7–11 July 2014, Boston, Mass.

Sheffield, A. M. (2016), Exploring post-cold frontal moisture transport in an idealized extratropical cyclone study. PhD Dissertation. Colorado State University. [Available at https://dspace.library.colostate.edu/handle/10217/100538/browse?type=author&value=Sheffield%2C+Amanda+Marie.]

Thompson, G., and T. Eidhammer (2014), A study of aerosol impacts on clouds and precipitation development in a large winter cyclone, *J. Atmos. Sci.*, *71*, 3636–3658.

Tselioudis, G., Y. Zhang, and W. B. Rossow (2000), Cloud and radiation variations associated with northern midlatitude low and high sea level pressure regimes, *J. Clim.*, *13*, 312–327.